AIP | The Journal of Chemical Physics

Analytical solution for the depolarization of hyperpolarized nuclei by chemical exchange saturation transfer between free and encapsulated xenon (HyperCEST)

Moritz Zaiss, Matthias Schnurr, and Peter Bachert

Citation: The Journal of Chemical Physics **136**, 144106 (2012); doi: 10.1063/1.3701178
View online: http://dx.doi.org/10.1063/1.3701178
View Table of Contents: http://scitation.aip.org/content/aip/journal/jcp/136/14?ver=pdfcov
Published by the AIP Publishing

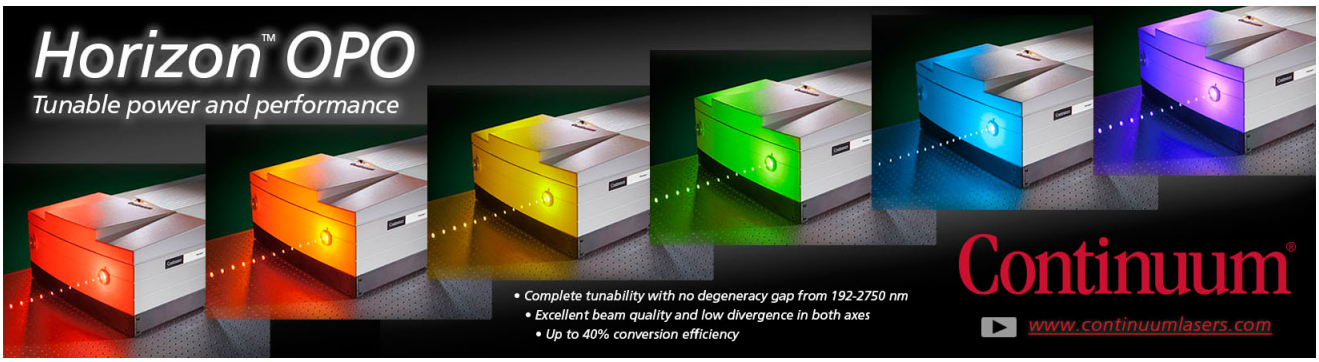

Analytical solution for the depolarization of hyperpolarized nuclei by chemical exchange saturation transfer between free and encapsulated xenon (HyperCEST)

Moritz Zaiss,[a] Matthias Schnurr, and Peter Bachert
Department of Medical Physics in Radiology, Deutsches Krebsforschungszentrum (DKFZ), Im Neuenheimer Feld 280, D-69120 Heidelberg, Germany

(Received 23 December 2011; accepted 20 March 2012; published online 10 April 2012)

We present an analytical solution of the Bloch–McConnell equations for the case of chemical exchange saturation transfer between hyperpolarized nuclei in cavities and in solvent (HyperCEST experiment). This allows quantitative investigation of host–guest interactions by means of nuclear magnetic resonance spectroscopy and, due to the strong HyperCEST signal enhancement, even NMR imaging. Hosts of interest can be hydrophobic cavities in macromolecules or artificial cages like cryptophane-A which was proposed as a targeted biosensor. Relevant system parameters as exchange rate and host concentration can be obtained from the monoexponential depolarization process which is shown to be governed by the smallest eigenvalue in modulus. For this dominant eigenvalue we present a useful approximation leading to the depolarization rate for the case of on- and off-resonant irradiation. It is shown that this rate is a generalization of the longitudinal relaxation rate in the rotating frame. We demonstrate for the free and cryptophane-A-encapsulated xenon system, by comparison with numerical simulations, that HyperCEST experiments are precisely described in the valid range of this widely applicable analytical approximation. Altogether, the proposed analytical solution allows optimization and quantitative analysis of HyperCEST experiments but also characterization and optimal design of possible biosensors. © *2012 American Institute of Physics*. [http://dx.doi.org/10.1063/1.3701178]

INTRODUCTION

Many enzymes bind to hydrophobic domains of substrate molecules to start a catalytic reaction. Without the substrate the domains are surrounded by water molecules. To get access to the non-polar domain, for the purpose to study physical properties such as shape, size, charge, and polarizability, the extrusion of the water molecules in the host molecule is required. The extrusion is only possible with a non-polar sensor as a guest in the host molecule, such as noble gases like ^{129}Xe.[1,2] Measurable quantities in nuclear magnetic resonance (NMR) spectroscopy, such as relaxation times, chemical shift, and spectral linewidth, are very sensitive to the chemical environment. A striking example is the Xe-protein host–guest interaction.[3] Due to the high polarizability of the ^{129}Xe electron cloud, which can be even more important than the strength of ligand binding,[4] ^{129}Xe is the adequate non-polar solute, and an ideal model to study hydrophobic interactions in aqueous solutions. Without changing the folding of proteins Xe is able to bind to intra- as well as inter-molecular sites and even enters small channel-like pore structures.[5]

Another advantage of ^{129}Xe (spin 1/2) is the feature that it can be hyperpolarized by laser-optical pumping.[6] The achieved population difference of the two Zeeman levels is several orders of magnitude larger than in thermal equilibrium. The resulting strong NMR signal enhancement allows to detect rare Xe in the sample.[7,8] In addition, chemical exchange of the small guest population with solute Xe can be used to transfer information to the larger solute Xe pool. Both phenomena require comprehensive evaluation of the manipulated solute Xe signal. This is what we analyze in the following.

Many different techniques to create non-thermal spin polarization have been invented, for example spin exchange optical pumping[6,9] (SEOP) to polarize the noble gases ^{3}He or ^{129}Xe, parahydrogen-induced polarization[10] (PHIP) of ^{13}C or ^{19}F in liquid phase, or dynamic nuclear polarization (DNP) of ^{13}C or ^{15}N in solid phase at cryogenic temperatures.[11] The degree of hyperpolarization for ^{129}Xe ranges from several percent[12,13] to up to 60%. Even higher values were obtained for ^{3}He using laser-optical pumping at low pressure and metastability exchange scattering.[14]

As an exemplary hydrophobic host for hyperpolarized Xe atoms we consider the molecular cage of cryptophane-A (CrA).[15] CrA can be utilized to detect specific biomolecules attached to CrA via molecular links to receptors.[16] Trapped hyperpolarized (hp) ^{129}Xe inside the cryptophane cage is labeled by means of selective radiofrequency (RF) saturation. The labeled state is then transferred to the solute Xe pool by chemical exchange. As a result, changes of the magnetization originating from caged Xe are strongly enhanced by accumulation in the much bigger solute pool. The combination of hp ^{129}Xe and chemical exchange saturation transfer (CEST)[17] is known as HyperCEST.[16] HyperCEST is a promising candidate for NMR detection of very small amounts of cages attached to target molecules *in vitro* and in tissue *in vivo*.

[a]Author to whom correspondence should be addressed. Electronic mail: m.zaiss@dkfz.de. Tel.: +49 6221-42 2543. FAX: +49 6221-42 3058.

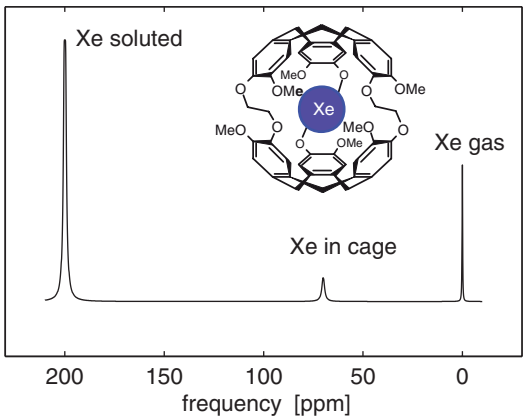

FIG. 1. Scheme of an ^{129}Xe NMR spectrum with resonances of Xe in the gas phase, in aqueous solution, and within dissolved cryptophane-A cages (inset courtesy Dr. Leif Schröder).

The pools in a HyperCEST experiment are the bulk aqueous phase pool of hyperpolarized ^{129}Xe, which is exchanging with one or more different cage pools (Fig. 1). After selective saturation of one cage pool with a long B_1 pulse, a signal loss in the bulk pool is observed due to the exchange of Xe atoms. Experiments showed that the overall attenuation of the hp Xe signal is monoexponential $\propto e^{-\lambda t}$, with depolarization decay rate $\lambda = \lambda_{depol}$.[18] The dependence of λ_{depol} on parameters which drive this depolarization, such as T_1 and T_2, the exchange rate k, the RF irradiation power, or the Xe and cage concentrations, is unknown.

The dynamics of exchanging spin systems is generally described by the Bloch–McConnell (BM) equations.[19] As shown by Ramirez *et al.*[20] HyperCEST experiments are well described by BM simulations. This encourages to derive an analytical expression for λ_{depol} by solving the BM differential equation system.

Here, we present an analytical solution for the BM dynamics of depolarization of an hp ensemble of nuclei in two exchanging pools. This general solution is applied to the experimentally realized system of ^{129}Xe spins in aqueous solution mixed with CrA cages. We show that the HyperCEST decay rate λ_{depol} measured in a depolarization experiment can be extended to a full solution by using input from direct saturation and CEST pool saturation. It turns out that λ_{depol} is a generalization of the longitudinal relaxation rate in the rotating frame $R_{1\rho}$ including chemical exchange. After verification by numerical BM simulations, this result and approximations on the one hand will be useful for determination of exchange rates and cage concentrations of a given HyperCEST system. On the other hand, it will enable optimal adjustment of cage properties for the design of highly specific biosensors.

THEORY

General approach to solve the BM equations governed by one dominant eigenvalue

We consider a system of two spin pools: *a* (free pool/spins in solution) and *b* (CEST pool/spins encapsulated in the cage molecule) undergoing chemical exchange, with thermal equilibrium magnetizations M_a^0 and M_b^0, respectively.

The dynamics of this 2-pool system under RF irradiation can be described classically with magnetization vectors $\vec{M}_a$ and $\vec{M}_b$ governed by the BM equations,[19] a coupled system of first-order linear differential equations. After transformation in the rotating frame of reference (x, y, z) the BM equations read

$$\frac{d}{dt}\begin{pmatrix} M_{ax} \\ M_{bx} \\ M_{ay} \\ M_{by} \\ M_{az} \\ M_{bz} \end{pmatrix} = \underbrace{\begin{pmatrix} -k_a - R_{2a} & k_b & -\Delta\omega_a & 0 & 0 & 0 \\ k_a & -k_b - R_{2b} & 0 & -\Delta\omega_b & 0 & 0 \\ \Delta\omega_a & 0 & -k_a - R_{2a} & k_b & -\omega_1 & 0 \\ 0 & \Delta\omega_b & k_a & -k_b - R_{2b} & 0 & -\omega_1 \\ 0 & 0 & \omega_1 & 0 & -k_a - R_{1a} & -k_b \\ 0 & 0 & 0 & \omega_1 & k_a & -k_b - R_{1b} \end{pmatrix}}_{\mathrm{A}} \cdot \begin{pmatrix} M_{ax} \\ M_{bx} \\ M_{ay} \\ M_{by} \\ M_{az} \\ M_{bz} \end{pmatrix} + R_1 \begin{pmatrix} 0 \\ 0 \\ 0 \\ 0 \\ M_a^0 \\ M_b^0 \end{pmatrix}. \tag{1}$$

In the rotating frame the RF irradiation field $\vec{B}_1 = (\omega_1/\gamma, 0, 0)$ is static. It rotates in the lab frame with the frequency ω_{rf}. Therefore, $\Delta\omega_{a/b} = \omega_{rf} - \omega_{a/b}$ is the irradiation frequency offset relative to the respective Larmor frequency $\omega_{a/b}$ of each pool. With the xenon gas peak (Larmor frequency ω_{gas}) as reference and $\Delta\omega = \omega_{rf} - \omega_{gas}$, the relative offset $\Delta\omega_{a/b}$ can be expressed by means of the chemical shift $\delta_i = \frac{\omega_i - \omega_{gas}}{\omega_{gas}}$ (of pool i = a, b), giving $\Delta\omega_{a/b} = \Delta\omega - \delta_{a/b} \cdot \omega_{gas} \equiv \Delta\omega - \delta\omega_{a/b}$. Let $\delta_{a/b} \cdot \omega_{gas} = \delta\omega_{a/b}$. $R_{1/2,a/b} = 1/T_{1/2,a/b}$ are the intrinsic relaxation rates of the pools. The coupling constants k_b, k_a are pseudo-first-order rate constants, which determine the chemical exchange for each direction of the transfer process (CEST pool → free pool and *vice versa*), given that the exchange of the two pools

obeys the rate equation in steady state

$$k_a = \frac{M_b^0}{M_a^0} k_b = f_b \times k_b, \tag{2}$$

where f_b is the concentration fraction. The BM equations, Eq. (1), are solved by finding the eigenvalues of the full rank matrix **A** leading to the general solution of the 2-pool system

$$\vec{\mathbf{M}}(t) = \sum_{n=1}^{6} e^{\lambda_n t} \vec{v}_n + \vec{S}, \tag{3}$$

where λ_n is the nth eigenvalue with the corresponding eigenvector $\vec{v}_n$ of **A** and $\vec{S}$ is the stationary solution. If the magnetization $\vec{\mathbf{M}}(t)$ is always much larger than $\vec{S}$, the stationary part can be neglected. This is the case in HyperCEST, because the hyperpolarization exceeds thermal polarization by a factor of up to 10^4. The dynamics is then described by the first term of Eq. (3).

Application of perturbation theory[21] yields two real eigenvalues and four complex eigenvalues; the real parts of all eigenvalues λ_n are negative. Without relaxation terms the first eigenvalue λ_1 is proportional to k_a and the corresponding eigenvector is oriented along the effective field $\vec{\omega}_{a,eff} = (\omega_1, 0, \Delta\omega_a)$ which is tilted by the angle $\theta = \tan^{-1}(\frac{\omega_1}{\Delta\omega_a})$ off the z axis of the rotating frame. For large chemical-shift differences the eigenvector of the smallest eigenvalue in modulus is closely aligned along the z-direction (0, 0, 1). The second eigenvalue λ_2 is proportional to k_b with corresponding eigenvector $\vec{\omega}_{b,eff} = (\omega_1, 0, \Delta\omega_b)$. All other eigenvalues contain terms $k_{a/b} \pm i\sqrt{\omega_1^2 + \Delta\omega_{a/b}^2}$ and are much larger in modulus than k_a (for complex eigenvalues "larger" refers to magnitudes).

We can therefore assume that all eigenvalues are much larger in modulus than the eigenvalue λ_1 (see Appendix). The fact that the eigenvector of this eigenvalue is closely aligned with M_z explains the observed monoexponential decay of M_z.[18] Consequently, we are looking for the smallest eigenvalue in modulus of the system. As shown in the Appendix, the smallest eigenvalue in modulus, i.e., λ_1, can generally be approximated by the first two coefficients c_0 and c_1 of the characteristic polynomial

$$\lambda_1 = -\frac{c_0}{c_1}, \tag{4}$$

which was suggested previously by Trott and Palmer.[24]

This fundamental result is employed in the following calculations.

Combined solution for HyperCEST

We derive the full solution for the decay of the free Xe magnetization observed in the HyperCEST experiment by separating the relaxation into two decay channels: The first channel is relaxation induced by exchange with the decaying CEST pool magnetization; relaxation of the free pool (pool *a*) is neglected. Likewise R_{1b}, which is assumed to be much smaller than k_b or R_{2b}, is not taken into account. The second channel is the depolarization process induced by direct saturation; here exchange with the CEST pool (pool *b*) is neglected. The superposition of these two channels is assumed to yield the full depolarization rate. This approach has the advantage of simpler mathematical expressions and is plausible if pool *b* is small ($f_b \ll 1$). In this case, exchange does not much alter the dominant direct water saturation dynamics ($\sim \sqrt{\Delta\omega_a^2 + \omega_1^2}$) and all direct relaxation of pool *a* are already modeled in first order. As a consequence we neglect direct relaxation of pool *a* in the exchange-induced depolarization process and disregard the relaxation rates R_{2a}, R_{1a}, and R_{1b} in matrix **A** to derive the depolarization rate λ_{CEST} induced by the CEST pool from Eq. (4) separately. This approach yields the full solution for the exchange-dependent depolarization rate

$$-\lambda_{CEST} = \frac{\omega_1^2 \frac{k_a \times k_b}{k_a + k_b} \times (\delta\omega_b - \delta\omega_a)^2 + \frac{R_{2b}}{k_a + k_b}\omega_1^2 k_a \left(\Delta\omega_a^2 + (k_a + k_b)^2 + k_b R_{2b} + \omega_1^2\right)}{(\Delta\omega_a(k_b + R_{2b}) + \Delta\omega_b k_a)^2 + (k_a + k_b + R_{2b})^2\omega_1^2 + (\Delta\omega_a\Delta\omega_b - k_a R_{2b})^2 + \Delta\omega_b^2\omega_1^2 + k_a R_{2b}\omega_1^2 + \frac{k_a + k_b + R_{2b}}{k_a + k_b}\left(\Delta\omega_a^2\omega_1^2 + \omega_1^4\right)}. \tag{5}$$

The solution of Eq. (4) for direct saturation without exchange terms is

$$-\lambda_{direct} = \frac{R_{1a}\Delta\omega_a^2 + R_{2a}\omega_1^2 + R_{1a}R_{2a}^2}{\Delta\omega_a^2 + \omega_1^2 + 2R_{1a}R_{2a}}. \tag{6}$$

This expression can be approximated by neglecting the longitudinal relaxation rate R_1 vs. rotation terms $\Delta\omega_a$ and ω_1 giving

$$-\lambda_{direct} = R_{1a}\cos^2\theta + R_{2a}\sin^2\theta. \tag{7}$$

Here again $\theta = \tan^{-1}(\frac{\omega_1}{\Delta\omega_a})$ is the angle between the z-axis and the tilted axis of the effective field $\vec{\omega}_{a,eff}$

$$\vec{\omega}_{a,eff} = \begin{pmatrix} \omega_1 \\ 0 \\ \Delta\omega_a \end{pmatrix}, \quad \omega_{a,eff} = \left|\vec{\omega}_{a,eff}\right| = \sqrt{\omega_1^2 + \Delta\omega_a^2}. \tag{8}$$

The superposition of depolarization of the CEST pool and direct saturation leads to the full analytical solution for

the HyperCEST depolarization rate λ_{depol} (which is a positive number)

$$\lambda_{depol} = -\lambda_{direct} - \lambda_{CEST}. \quad (9)$$

The model function for the normalized z-spectrum, i.e., the z-magnetization after preparation Z_{prep}, normalized by the longitudinal magnetization of pool a M_{za} at $t = 0$, reads

$$Z_{prep}(\Delta\omega) = \frac{M_{za}(t_{sat})}{M_{za}(t=0)}(\Delta\omega) = e^{-\lambda_{depol}(\Delta\omega)t_{sat}}. \quad (10)$$

Z_{prep} represents the NMR signal after preparation

$$\frac{\text{NMR signal after irradiation at } \Delta\omega}{\text{NMR signal without irradiation}} = Z_{prep}(\Delta\omega). \quad (11)$$

If direct saturation is neglected, the HyperCEST effect can be defined appropriately as

$$\text{HyperCEST} = 1 - Z_{prep}(\Delta\omega). \quad (12)$$

Approximative solutions for HyperCEST

The chemical-shift difference $|\delta_a\text{-}\delta_b|$ for free xenon and xenon in cages is larger than 100 ppm.[22] Therefore, both terms of direct saturation in Eq. (7) are approximately constant at the CEST resonance. With the assumptions $|\delta_a\text{-}\delta_b| \gg 1$ and $k_a \ll k_b$ the HyperCEST depolarization rate λ_{depol} has a Lorentzian line shape as a function of $\Delta\omega_b$. This is seen when only leading terms of the Taylor series in k_a are considered which yields the following approximation for Eq. (9):

$$\lambda_{depol} = C + L(\lambda_{max}, \Gamma, \Delta\omega) = C + \frac{\lambda_{max} \cdot \frac{\Gamma^2}{4}}{\frac{\Gamma^2}{4} + (\Delta\omega_b - x_0)^2}. \quad (13)$$

The first term in Eq. (13) equals Eq. (7), i.e., $C = -\lambda_{direct}$, and reads

$$C = R_{1a}\cos^2\theta + R_{2a}\sin^2\theta. \quad (14)$$

The quantities that characterize the Lorentzian $L(\lambda_{max}, \Gamma, \Delta\omega)$ in Eq. (13) are maximum λ_{max} (a linear function of k_a [Eq. (15)]), full-width at half-maximum (FWHM) Γ , and frequency shift x_0 away from δ_b

$$\lambda_{max} = \sin^2\theta \cdot k_a \cdot \frac{(\delta\omega_b - \delta\omega_a)^2 + k_b R_{2b} + \frac{R_{2b}}{k_b + R_{2b}} \cdot \omega_1^2}{\omega_1^2 + k_b(k_b + R_{2b})} \overset{(\delta\omega_b - \delta\omega_a) \gg R_{2b}, k_b, \omega_1}{\approx} \frac{k_a \cdot \omega_1^2}{\omega_1^2 + k_b(k_b + R_{2b})}, \quad (15)$$

$$\Gamma = 2\sqrt{\frac{k_b + R_{2b}}{k_b} \cdot \omega_1^2 + (k_b + R_{2b})^2}, \quad (16)$$

$$x_0 = \frac{(\delta\omega_b - \delta\omega_a)k_a k_b}{\omega_1^2 + (\delta\omega_b - \delta\omega_a)^2}. \quad (17)$$

Solving Eq. (10) for the depolarization rate shows how λ_{depol} can be obtained from experimental data:

$$\lambda_{depol} = -\frac{\log(Z_{prep}(\Delta\omega))}{t_{sat}}. \quad (18)$$

This means that not the prepared z-magnetization, but its logarithm follows a Lorentzian lineshape.

If R_{2b} is neglected vs. k_b and ω_1 in Eqs. (15) and (16) and assuming $k = (k_a + k_b) \sim k_b$ we obtain the asymmetric population limit of $R_{1\rho}$ found for spinlock experiments[23]

$$\lambda_{depol} = R_{1\rho} = R_{1a}\cos^2\theta + R_{2a}\sin^2\theta + \sin^2\theta \cdot \frac{\frac{k_a \cdot k_b}{k^2} \cdot (\delta\omega_b - \delta\omega_a)^2 \cdot k}{\Delta\omega_b^2 + \omega_1^2 + k^2}. \quad (19)$$

This is again a Lorentzian line with the same baseline C as in Eq. (13), but maximum and linewidth different from Eqs. (15) and (16)

$$\lambda_{max} = \sin^2\theta \cdot \frac{\frac{k_a \cdot k_b}{k^2} \cdot (\delta\omega_b - \delta\omega_a)^2 \cdot k}{\omega_1^2 + k^2}, \quad (20)$$

$$\Gamma = 2\sqrt{\omega_1^2 + (k_a + k_b)^2}. \quad (21)$$

MATERIAL AND METHODS

All simulations were performed with MATLAB 7 (The Mathworks, Natick, MA, USA) assuming a static magnetic field $B_0 = 9.4$ T and Xe spin pools resonating at chemical shifts $\delta_a = 200$ ppm (solute pool a) and $\delta_b = 70$ ppm (CEST pool b) relative to the Xe gas peak at $\delta = 0$ ppm. Its Larmor frequency is $\omega_{gas} = \gamma B_0 = 726.6$ MHz ($\gamma/2\pi = 11.8$ MHz/T).

Numerical solution

The dynamics of the magnetization vectors of the spin pools were calculated by means of the numerical BM matrix solution introduced by Woessner *et al.*[24] Simulation parameters were chosen according to published data.[15,18,25]

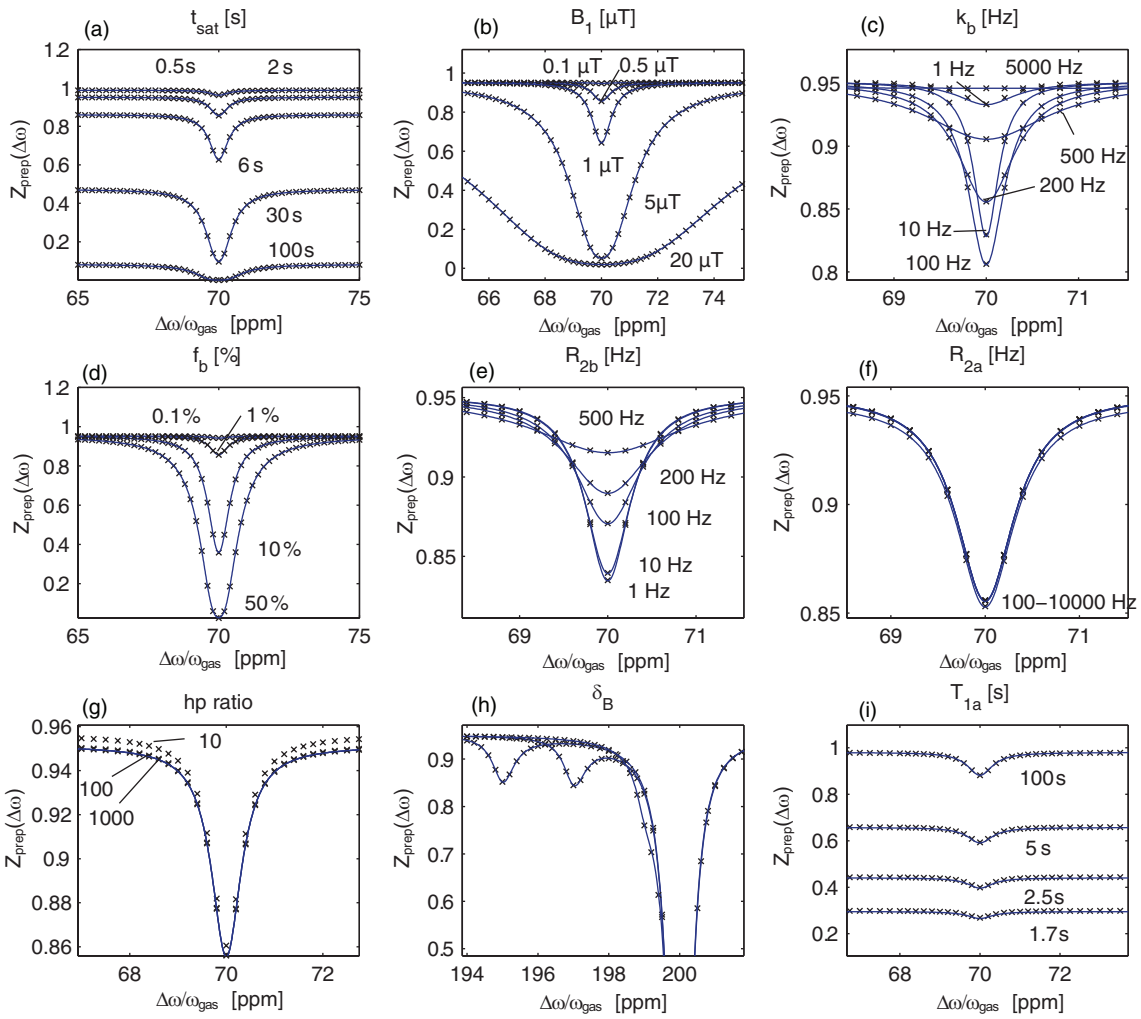

FIG. 2. Theoretical z-spectra for HyperCEST demonstrate high correlation between analytical (solid line) and numerical solution (crosses) for all observed parameter values and all observed off-resonances. Depolarization increases with increasing saturation time t_{sat}, RF field amplitude B_1, and concentration fraction f_b (a, b, d). With increasing k_b (c) depolarization increases, attains a maximum and decreases for high k_b as well as for large R_{2b} (e). The relaxation of the free pool affects only the baseline of the CEST peak (f, i). A hyperpolarization > 100 × thermal polarization is mandatory for the model to match the simulation (g). (h) displays the agreement of model and simulation with the direct saturation of free pool, but also demonstrates that the model is able to describe the spillover dilution of the CEST peak properly. Numerical evaluation of the full BM equations employed the modified model of Woessner *et al.*[24] and took ∼5 ms per z-spectrum.

Hence the longitudinal relaxation time in both pools was set to $T_{1a} = T_{1b} = 40$ s, the transversal relaxation time in pool *a* to $T_{2a} = 50$ ms, and the concentration fraction was normalized by pool *a* to $f_a = M_a^0/M_a^0 = 1$ and $f_b = M_b^0/M_a^0$. The following parameters were varied separately: k_b, f_b, R_{2a} and R_{2b}, R_{1a} and R_{1b}, δ_b, and the ratio of hyperpolarization to thermal polarization. k_a was derived from Eq. (2).

The z-spectra were simulated with a sampling increment of 0.1 ppm between 60 and 80 ppm assuming continuous-wave (CW) saturation with amplitude B_1 chosen from the range between 0.1 and 20 μT at different saturation times t_{sat}. If not varied, the standard parameters used were $B_1 = 0.5$ μT, $t_{sat} = 2$ s, $R_{1a} = R_{1b} = 0.025$ Hz, $R_{2a} = 20$ Hz, $R_{2b} = 50$ Hz, $f_b = 1\%$, $k_{ba} = 200$ Hz. The degree of hyperpolarization was set to 5% ($\cong 5 \times 10^4$ times the thermal polarization). The time needed for the simulation of one z-spectrum was ∼5 ms.

Analytical solution

The simulations of z-spectra and the full solution Eq. (5) were plotted in the same diagram. The simulated z-spectra were fitted with Lorentzian lineshapes and the resulting linewidth Γ_{fit} was plotted together with the theoretical Γ of Eq. (16). The theoretical maximum of the Lorentzian λ_{max}, Eq. (15), together with the baseline C in Eqs. (13) and (14), were used to calculate an approximate Z_{prep} which was plotted together with the full solution and the numerical simulation for the case of resonant irradiation on the CEST pool.

RESULTS

The analytical z-spectra obtained with Eq. (10) coincide with simulated z-spectra for different saturation times t_{sat} (Fig. 2(a)) and amplitudes B_1 of the saturation pulse trains

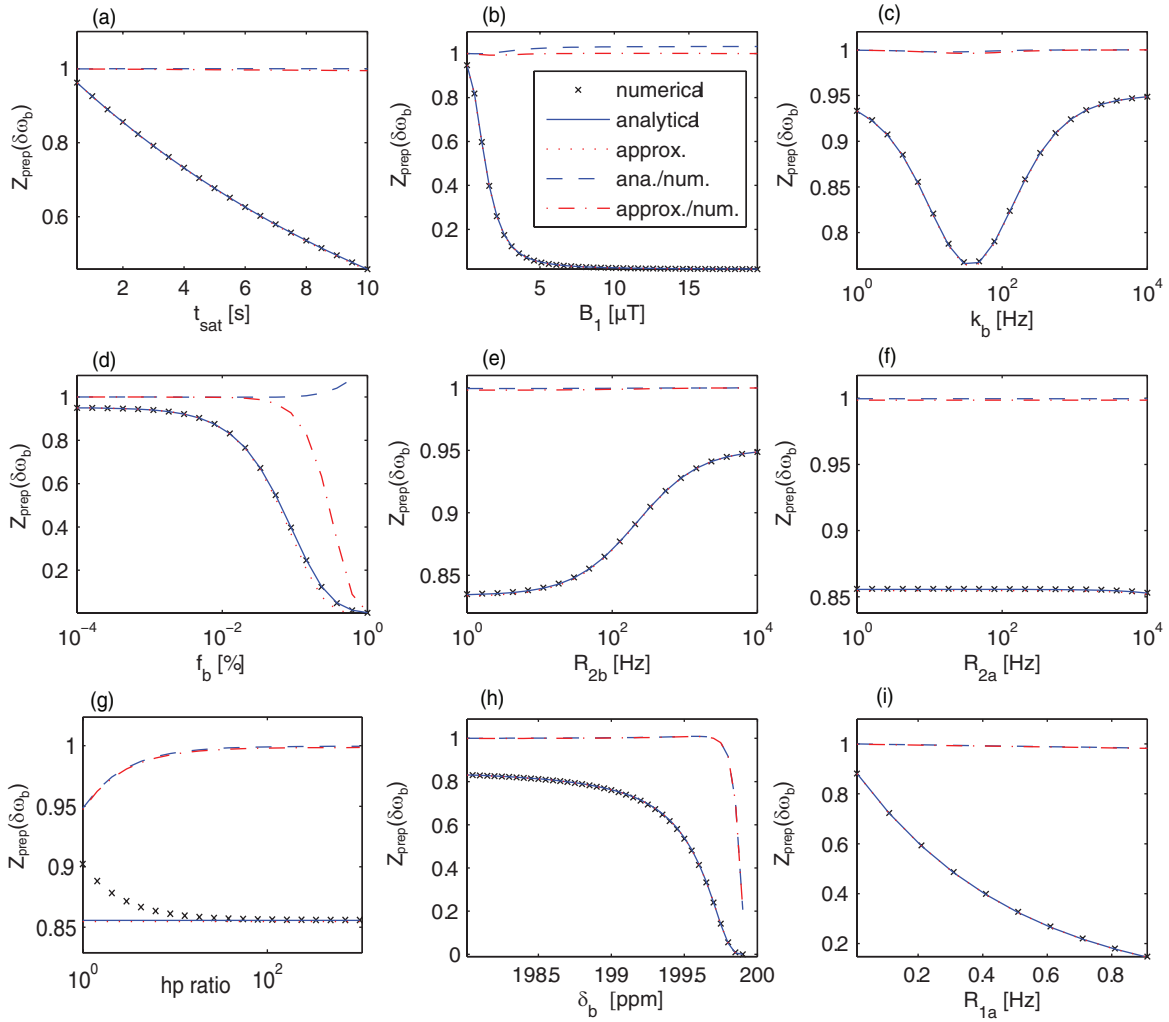

FIG. 3. The normalized z-magnetization after preparation $Z_{prep}(\delta\omega_b = \omega_{gas} \cdot 70$ ppm = CEST-resonant) shows high correlation between the full analytical solution [Eq. (9), solid], the approximate Lorentzian solution [Eq. (13), dotted], and the numerical solution (crosses) for all observed parameter values. (a) demonstrates the monoexponential decay $\sim\exp(-t_{sat} \times \lambda_{depol})$ of Z_{prep} with damping constant λ_{depol}. The depolarization increases with increasing field amplitude B_1 (b). The optimal exchange rate found for the standard parameters (see Methods) was $k_b \sim 35$ Hz (c). Z_{prep} decreases with increasing f_b (d). The depolarization process becomes inefficient for large R_{2b} (e). R_{2a} apparently has no influence on the CEST-resonant depolarization (f); the same is observed for sufficiently large hyperpolarization (> 100 × thermal polarization) (g). With smaller chemical shift (h), and also shorter T_1 times (i), direct saturation becomes more efficient and dominates the depolarization process. The ratios of results from the analytic model and the simulation are plotted for the full model (dashed) and the approximate Lorentzian maximum (dash-dotted). Both are close to 1 if $B_1 < 5\ \mu$T, $f_b < 50\%$ (full solution) or $f_b < 10\%$ (approx. solution), hyperpolarization > 100 × thermal polarization, and chemical shift > 0.5 ppm for the standard parameters.

(Fig. 2(b)). Analytical solution and numerical simulation also match well when k_b is varied in the range between 1 Hz and 5000 Hz (Fig. 2(c)): The CEST effect increases initially with increasing k_b, then attains a maximum and finally decreases caused by exchange-dependent linebroadening. Only for very small exchange rates ($k_b < 5$ Hz) the width of the z-spectra around the CEST pool deviates from the numerical solution. With increasing concentration fraction f_b both solutions consistently yield the increase of the CEST effect up to 50% relative concentration (Fig. 2(d)). On the other hand, the matching range goes down to $f_b = 0.001\%$ (data not shown).

Simulated z-spectra for varying R_{2b} (Fig. 2(e)) also fit well and show similar effects on linewidth and maximum of the CEST peak as f_b and k_b. This is an important observation, because it shows that the parameters R_{2b}, f_b, and k_b cannot be determined separately from one single z-spectrum. Changes in R_{2a} have a negligible effect on the z-spectrum (Fig. 2(f)) whereas $R_{1a} = 1/T_{1a}$ influences mainly the baseline of the z-spectrum (Fig. 2(i)). Simulations with smaller degree of hyperpolarization showed that hp of more than 100 times the thermal polarization is sufficiently far away from the stationary solution (Fig. 2(g)). The outcome is surprising when the chemical-shift difference of CEST and free pool is only a few ppm (Fig. 2(h)): the theory describes not only the dynamics of the free pool accurately, but also the dilution of the CEST peak by direct saturation (spillover effect) is modeled with high precision.

Analytical z-spectra that match well with the full numerical solution demonstrate the validity of the model function (Eq. (9)) in the off-resonant case for all parameters in the observed range.

For a detailed investigation of the range of validity of the solution $Z_{prep} = \exp(-\lambda_{depol} \cdot t_{sat})$ [Eq. (10)] and of its "Lorentzian approximation" with maximum λ_{max}, Eq. (15)

$Z_{prep} \cong \exp[-(C+\lambda_{max}) \cdot t_{sat}]$ we examined the normalized z-magnetization after preparation $Z_{prep}(\delta_b)$ for the case of on-resonant irradiation on the CEST pool.

The on-resonant monoexponential decay observed in simulations turned out to match the analytical expression with only a small relative error (dashed and dash-dotted line Fig. 3(a)). $Z_{prep}(\delta\omega_b)$ as a function of the RF irradiation amplitude B_1 is exact up to $B_1 = 1\ \mu$T. For larger B_1-fields there is a deviation of ~5% (Fig. 3(b)) which is possibly caused by proximity to the stationary regime in the case of high power. The deviation of the Lorentzian approximation ($Z_{prep} \cong \exp[-(C+\lambda_{max}) \cdot t_{sat}]$) from the simulated data is even smaller than the deviation of the full solution.

$Z_{prep}(\delta\omega_b)$ as a function of k_b also matches well for exchange rates in the range of 1 Hz–10^{10} Hz. This means that the model is valid for slow *and* fast exchange (Fig. 3(c)). For the standard parameters (see Methods section) an optimal exchange rate $k_{b,opt} \approx 35$ Hz is observed for all analytical and numerical solutions. Accordingly, $k_{b,opt}$ can be predicted by minimization of Eq. (15). The analytical prediction of Z_{prep} as a function of the concentration fraction f_b is suitable only up to $f_b \approx 50\%$ for the full solution and up to $f_b \approx 10\%$ for the Lorentzian approximation (Fig. 3(d)). For the full solution this again can be caused by approach to the stationary solution, because depolarization increases with concentration fraction. Our simulations showed that a decrease of the saturation time t_{sat} also reduces the deviation from analytical solutions for large f_b. For the Lorentzian approximation we took the Taylor series to first order in k_a. This leads to a model which is only valid for $k_a \ll 1$.

Both the analytical solution for the depolarization of Eqs. (5) and (6) as well as the approximation $Z_{prep} \cong \exp[-(C+\lambda_{max}) \cdot t_{sat}]$ (Eqs. (15) and (18)) predict the dependence of HyperCEST on the relaxation rates R_{2b}, R_{2a}, and R_{1a} with high precision (Fig. 3(e), 3(f), and 3(i)), except for too high R_{1a}: In this case there is a deviation owing to a faster depolarization towards the stationary solution $\vec{S}$ [Eq. (3)].

The results displayed in Fig. 3 demonstrate that the range of validity of the presented model is very large. The main requirements concerning Z_{prep} on the CEST resonance are

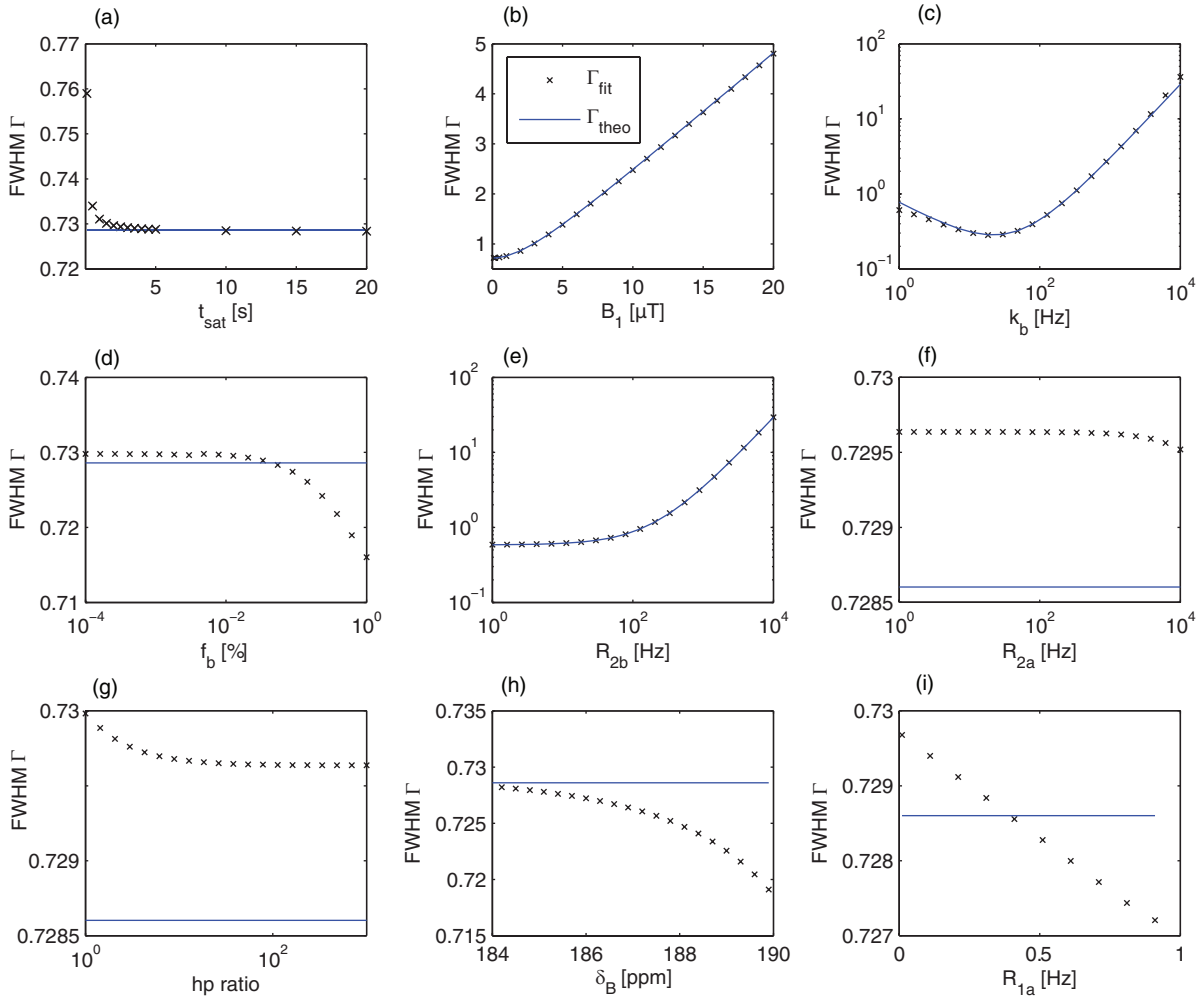

FIG. 4. Linewidth (FWHM) Γ of $\lambda_{depol} = -\log(Z_{prep})/t_{sat}$ as a function of varied parameters. Crosses mark Γ_{fit} of the Lorentzian fit of Eq. (13); the solid line represents the analytical term Γ_{theo} of Eq. (15). The Lorentzian fit yielded high correlation $R^2 > 99.96\%$ for all parameters except δ_b. The expected Γ_{theo} matched Γ_{fit} within 5% error for $t_{sat} > 0.1$s (a), all values of B_1 in the range 0–20 μT (b), 10 Hz < k_b < 2000 Hz (c) and all observed f_b, R_{2b}, R_{2a}, hyperpolarization and R_{1a} (d, e, f, g, i). For small chemical shift difference $|\delta_b - \delta_a|$ the Lorentzian fit was inappropriate, because the baseline of Eq. (7) is not constant anymore. Γ_{theo} does not depend on f_b, R_{2a} and R_{1a}, but the deviation from Γ_{fit} for realistic parameter values is small. Note the minimum of FWHM at $k_b \sim 20$ Hz (c). This is near the maximum effect in Fig. 3(c) and therefore optimal for effective depolarization and narrow lines for a specific saturation scheme.

sufficiently high degree of polarization ($\approx$>100 × thermal polarization), low concentration fraction (<5%), and sufficiently long T_1 relaxation time (>2 s). These constraints arise from the approach to the stationary solution of Eq. (3). Hence, for a given system t_{sat} and B_1 can be adjusted such that M_z remains in the regime far away from stationary conditions.

The examination of the width Γ_{fit} of Lorentzian lineshapes fitted to $-\log(Z_{prep}(\Delta\omega))/t_{sat}$ (Eq. (18)) using the numerical simulation showed that Γ_{fit} follows in good approximation the theoretical linewidth (FWHM) Γ_{theo} in Eq. (16). From Fig. 4 the domain can be estimated where Γ_{theo} matches Γ_{fit} within 5% error and thus the evaluation of z-spectra using the model of Lorentzian lineshapes is appropriate. For the standard parameters this range is given by $t_{sat} > 0.1$ s, 10 Hz < k_b < 2000 Hz, δ_a–δ_b > 5 ppm. All other parameters can be chosen arbitrarily.

Regarding FWHM as a function of k_b, a minimum is found at $k_b \sim 20$ Hz (Fig. 4(c)). Together with the maximum effect in Fig. 3(c) an optimal exchange rate can then be defined that yields a strong depolarization effect, but a narrow line for a specific saturation scheme.

The results shown in Figs. 3 and 4 demonstrate that the Lorentzian line analysis of z-spectra based on Eq. (13) is valid and appropriate for systems with parameters λ_{max} and Γ within the discussed ranges. The measurement of Γ as a function of B_1 allows to determine quantitatively the rate constants k_b and R_{2b} available and consequently, by use of λ_{max}, one also obtains f_b.

Thus the HyperCEST effect in the case of resonant irradiation on the CEST pool is given by the simple approximation (Eqs. (10) and (12), and (14))

$$\text{HyperCEST} = 1 - \exp\left(-\left[R_{1a} + \frac{k_a \cdot \omega_1^2}{\omega_1^2 + k_b(k_b + R_{2b})}\right] \cdot t_{sat}\right). \quad (22)$$

If R_{2b} is negligible, f_b and k_b can be obtained separately by taking advantage of λ_{max} of Eq. (20) and Γ of Eq. (21).

Even without matching of C, λ_{max}, and Γ_{fit}, which means leaving the valid range of our approximation, the Lorentzian fit was always possible with high $R^2 > 99.96\%$ for all parameters, except δ_b. This means that the full λ_{depol} can be described by a Lorentzian lineshape in all observed parameter ranges. For small chemical-shift differences, C is not constant and a single Lorentzian fit is not possible. However, a superposition of Lorentzian lines is appropriate as demonstrated in Fig. 2(h): the superposed λ_{depol} describes the data well even for small chemical-shift differences.

DISCUSSION

The exchange between spin pools monitored in a CEST experiment can alternatively be measured in a spinlock (SL) experiment.[26] In the SL experiment, the z-magnetization of one pool is first turned by 90° into the x–y plane of the rotating frame and immediately afterwards spinlocked along the y axis by a 90°-phase-shifted on- or off-resonant RF pulse. The locked magnetization decays exponentially with the longitudinal relaxation time in the rotating frame, $T_{1\rho}$, to the new thermal equilibrium magnetization defined by the field B_1, which is static in the rotating frame. Since $B_1 \ll B_0$, the locked magnetization is much larger than the thermal equilibrium magnetization along B_1, hence the spin system is hyperpolarized. This analogy of spinlock and hyperpolarization explains that HyperCEST experiments can be understood as SL experiments, but conversely SL can also be understood as a hyperpolarization experiment. This immediately allowed the use of the existing spinlock approaches for exchanging spin systems described by the BM equations.

The SL approach of Trott and Palmer[23] was justified by neglecting higher-order terms in the characteristic polynomial. This was revised by other approaches, one using perturbation theory[21] and another using the Laguerre approximation for the smallest root of a polynomial.[28]

Our trials to extend the perturbation theory approach by R_{2b} were unsuccessful. Therefore, the original approximation[23] was resumed by inspection of the coefficients c_0 and c_1 instead of the argument in the characteristic polynomial. Our ansatz leads to similar results as approaches employing a Laguerre approximation[28] or the Laplace transformation.[29] It is important to note that our derivation explains why the approximation in Eq. (4) is valid: The smallest eigenvalue in modulus must be much smaller than all others! This means on the other hand: if the decay of the magnetization is actually monoexponential then one eigenvalue of the solution of the BM equations dominates and therefore our approach is valid.

We extended the Bloch–McConnell matrix **A** of Trott and Palmer[23] by choosing two different transversal relaxation times R_{2a} and R_{2b} to model the linebroadening resulting from R_{2b} of the CEST pool. In previous publications[4,21,23,28–30] R_2 of the exchanging pools was neglected and for the free pool average values of transversal relaxation rates weighted by the concentration fraction were used. Now we could show that R_{2b} has a strong effect on the maximum and width of a CEST peak. Therefore, our generalized approach leads to a model which includes R_{2b} and which is also valid for SL experiments. Recently, it has been demonstrated that the steady-state can be also taken into account; this allows the application of the presented treatment also to non-hyperpolarized magnetization transfer experiments.[27]

With access to the dependence of the linewidth on R_{2b}, the rates R_{2b} and k_b can now be determined by means of Eq. (15). If the values of R_{2b} and k_b are known, f_b can be determined via Eq. (15) which is linear in $k_a = f_b \cdot k_b$.

This is to our knowledge the first theoretical treatment which provides quantitative access to HyperCEST experiments. By means of this quantification it is possible to predict exchange rates of HyperCEST agents and thus their dependence on temperature by the influence of the RF amplitude B_1 on the z-spectrum.

The shift $x_0 = \frac{(\delta\omega_b - \delta\omega_a)k_a k_b}{\omega_1^2 + (\delta\omega_b - \delta\omega_a)^2}$ (Eq. (17)) becomes important in the fast exchange limit ($k_b > (\delta_b - \delta_a)$). In the case of ^{129}Xe at $B_0 = 9.4$ T, an exchange rate $k_b = 1000$ Hz, and $f_b = 1\%$, the resulting shift x_0 of the CEST peak is about 0.02 ppm. The application of this effect to determine system parameters will be discussed in a forthcoming paper.

The model was also able to describe z-spectra correctly even in the case of very small chemical shifts of the pool (Fig. 2). This means that the case of spillover which is a central problem in proton CEST (Refs. 31 and 32) is treated effectively by the proposed model and the interferences of CEST and solute pool are described correctly. By means of our extended model the question may be answered whether or not the assumed pseudo-first-order treatment of the exchange process is valid for encapsulated Xe systems.

By quantitative understanding of the xenon-cryptophane depolarization the transfer of the HyperCEST experiment to more complicated "cages"[1,2] is prepared.

CONCLUSION

In this study, a general approximate approach for solution of the BM equations was found. It assumes that one eigenvalue is much smaller in modulus than all others. This was shown to be valid for the HyperCEST system. The decay rate λ_{depol} of the z-magnetization during irradiation was obtained by combination of the dominant eigenvalues of direct saturation (λ_{direct}) and CEST pool irradiation (λ_{CEST}). The theory was verified by numerical simulations and explains the monoexponential decay of z-magnetization observed in HyperCEST experiments. The presented Lorentzian approximation will allow a straightforward evaluation of experimental data within a large range of valid system parameters including R_{2b}, which is difficult of access. A surprising outcome is that λ_{depol} corresponds to the longitudinal relaxation rate in the rotating frame $R_{1\rho}$ observed in spinlock experiments. Conversely, our approach is a generalization of $R_{1\rho}$, i.e., extended by R_{2b}, and also applicable to the analysis of SL experiments. The theoretical solution allows quantification of HyperCEST experiments and by this means an appropriate design of biosensors but also access to kinetics of other hyperpolarized nuclei within hydrophobic hosts.

ACKNOWLEDGMENTS

We gratefully thank Dr. Leif Schröder, Jörg Döpfert, and Martin Kunth for helpful discussions.

APPENDIX: DERIVATION OF THE EIGENVALUE APPROXIMATION

The eigenvalues are the root of the normalized characteristic polynomial defined by

$$\mathrm{Det}(A-\lambda I)=0 \Leftrightarrow \lambda^n + c_{n-1}\lambda^{n-1} + .. + c_1\lambda^1 + c_0 = 0, \tag{A1}$$

where[33]

$$c_0 = \mathrm{Det}(A) \tag{A2}$$

and

$$c_1 = (-1)^1 \sum_{i=1}^{n} \mathrm{Det}(A_{ii}). \tag{A3}$$

The minor A_{ii} is obtained by by removing the ith column and ith row of matrix A. Because the determinant and the characteristic polynomial are independent of the basis, we choose a basis of eigenvectors where A_{ii} is diagonal. In the eigenbasis it is easy to see that Det(A) is the product of the eigenvalues

$$c_0 = \mathrm{Det}(A) = \lambda_1 \cdot \ldots \cdot \lambda_n \tag{A4}$$

and

$$c_1 = (-1)\sum_{i=1}^{n} \mathrm{Det}(A_{ii}) = -\sum_{i=1}^{n} \frac{\lambda_1 \cdot \ldots \cdot \lambda_n}{\lambda_i}$$

$$= -\mathrm{Det}(A) \cdot \sum_{i=1}^{n} \frac{1}{\lambda_i}. \tag{A5}$$

The assumption that all eigenvalues are much larger in modulus than λ_1

$$|\lambda_1| \ll |\lambda_2| \le |\lambda_3| \le \ldots \le |\lambda_n| \tag{A6}$$

leads to

$$c_1 = -\mathrm{Det}(A) \cdot \left(\frac{1}{\lambda_1} + \frac{1}{\lambda_2} + \ldots \frac{1}{\lambda_n}\right) \approx -\frac{\mathrm{Det}(A)}{\lambda_1}. \tag{A7}$$

This approximation is also valid for complex eigenvalues, because the conjugate complex is also an eigenvalue and therefore,

$$\frac{1}{\lambda_j} + \frac{1}{\lambda_j^*} = \frac{2\Re(\lambda_j)}{|\lambda_j|^2} \le \frac{2}{|\lambda_j|}. \tag{A8}$$

Equations (A4) and (A5) together with assumption (A6) allow that the smallest eigenvalue in modulus can generally be approximated by

$$\lambda_1 = -\frac{c_0}{c_1}. \tag{A9}$$

[1] C. Landon, P. Berthault, F. Vovelle, and H. Desvaux, Protein Sci. **10**, 762 (2001).
[2] A. Cherubini and A. Bifone, Prog. Nucl. Magn. Reson. Spectrosc. **42**, 1 (2003).
[3] R. F. Tilton and I. D. Kuntz, Biochemistry **21**, 6850 (1982).
[4] M. L. Quillin, W. A. Breyer, I. J. Griswold, and B. W. Matthews, J. Mol. Biol. **302**, 955 (2000).
[5] T. Prangé, M. Schiltz, L. Pernot, N. Colloc'h, S. Longhi, W. Bourguet, and R. Fourme, Proteins **30**, 61 (1998).
[6] T. G. Walker and W. Happer, Rev. Mod. Phys. **69**, 629 (1997).
[7] X. Zeng, C. Wu, M. Zhao, S. Li, L. Li, X. Zhang, Z. Liu, and W. Liu, Chem. Phys. Lett. **182**, 538 (1991).
[8] D. Raftery, H. Long, T. Meersmann, P. J. Grandinetti, L. Reven, and A. Pines, Phys. Rev. Lett. **66**, 584 (1991).
[9] M. A. Bouchiat, T. R. Carver, and C. M. Varnum, Phys. Rev. Lett. **5**, 373 (1960).
[10] L. T. Kuhn, U. Bommerich, and J. Bargon, J. Phys. Chem. A **110**, 3521 (2006).
[11] J. H. Ardenkjær-Larsen, B. Fridlund, A. Gram, G. Hansson, L. Hansson, M. H. Lerche, R. Servin, M. Thaning, and K. Golman, Proc. Natl. Acad. Sci. U.S.A. **100**, 10158 (2003).
[12] F. W. Hersman, I. C. Ruset, S. Ketel, I. Muradian, S. D. Covrig, J. Distelbrink, W. Porter, D. Watt, J. Ketel, J. Brackett, A. Hope, and S. Patz, Acad. Radiol. **15**, 683 (2008).
[13] I. C. Ruset, S. Ketel, and F. W. Hersman, Phys. Rev. Lett. **96**, 053002 (2006).
[14] J. Rivoire, M. Terekhov, F. M. Meise, K. Gast, Z. Salhi, and L. M. Schreiber, Magn. Reson. Med. **65**, 399 (2011).
[15] M. M. Spence, S. M. Rubin, I. E. Dimitrov, E. J. Ruiz, D. E. Wemmer, A. Pines, S. Q. Yao, F. Tian, and P. G. Schultz, Proc. Natl. Acad. Sci. U.S.A. **98**, 10654 (2001).
[16] L. Schröder, T. J. Lowery, C. Hilty, D. E. Wemmer, and A. Pines, Science **314**, 446 (2006).

[17]K. Ward, A. Aletras, and R. Balaban, J. Magn. Reson. **143**, 79 (2000).
[18]L. Schröder, L. Chavez, T. Meldrum, M. Smith, T. J. Lowery, D. E. Wemmer, and A. Pines, Angew. Chem., Int. Ed. **47**, 4316 (2008).
[19]H. M. McConnell, J. Chem. Phys. **28**, 430 (1958).
[20]R. M. Ramirez, T. K. Stevens, M. A. Smith, D. E. Wemmer, and A. Pines, Proceedings of ISMRM 19th Annual Meeting, Montreal, 2011, Vol. 19, p. 3542.
[21]O. Trott and A. G. Palmer III, J. Magn. Reson. **170**, 104 (2004).
[22]L. Schröder, T. Meldrum, M. Smith, T. J. Lowery, D. E. Wemmer, and A. Pines, Phys. Rev. Lett. **100**, 257603 (2008).
[23]O. Trott and A. G. Palmer III, J. Magn. Reson. **154**, 157 (2002).
[24]D. E. Woessner, S. Zhang, M. E. Merritt, and A. D. Sherry, Magn. Reson. Med. **53**, 790 (2005).
[25]T. Meldrum, L. Schröder, P. Denger, D. E. Wemmer, and A. Pines, J. Magn. Reson. **205**, 242 (2010).
[26]T. Jin, J. Autio, T. Obata, and S. Kim, Magn. Reson. Med. **65**, 1448 (2011).
[27]M. Zaiss and P. Bachert, e-print arXiv:1203.2067.
[28]V. Z. Miloushev and A. G. Palmer III, J. Magn. Reson. **177**, 221 (2005).
[29]D. Abergel and A. G. Palmer, ChemPhysChem **5**, 787 (2004).
[30]O. Trott, D. Abergel, and A. G. Palmer, Mol. Phys. **101**, 753 (2003).
[31]M. Zaiss, B. Schmitt, and P. Bachert, J. Magn. Reson. **211**, 149 (2011).
[32]P. Z. Sun and A. G. Sorensen, Magn. Reson. Med. **60**, 390 (2008).
[33]E. Peschl, *Analytische Geometrie und lineare Algebra* (Bibliographisches Institut, Mannheim, 1964), p. 102.